PHOTONICS Research

Mode selection and dispersion engineering in Bragg-like slot photonic crystal waveguides for hybrid light–matter interactions

Samuel Serna, Weiwei Zhang, Thi Hong Cam Hoang, Carlos Alonso-Ramos, Delphine Marris-Morini, Laurent Vivien, and Eric Cassan*

Centre de Nanosciences et de Nanotechnologies, UMR 9001 (CNRS/Université Paris-Sud), Université Paris-Saclay, 91405 Orsay, France
**Corresponding author: eric.cassan@u-psud.fr*

Received 4 July 2017; revised 21 November 2017; accepted 21 November 2017; posted 22 November 2017 (Doc. ID 301359); published 22 December 2017

We introduce a family of slot photonic crystal waveguides (SPhCWs) for the hybrid integration of low-index active materials in silicon photonics with energy-confinement factors of ∼30% in low-index regions. The proposed approach, which is based on a periodic indentation of the etched slot in the middle of the SPhCW, makes it possible to reconcile a simultaneously narrow and wide slot for exploiting the two modes of even symmetry of a SPhCW. The resulting mode-selection mechanism allows a flexible choice of the modes to be used. Furthermore, the proposed structure offers tremendous flexibility for adjusting the dispersive properties of the slot-confined modes, in particular of their slow-light effects. Flat band slow light in a bandwidth of about 60 nm with a group velocity dispersion factor $|\beta_2|$ below 1 ps^2/mm is numerically demonstrated by this approach, corresponding to a normalized delay bandwidth product of around 0.4. These results, obtained from hollow-core periodic waveguides that are directly designed in view of hybrid integration of active materials in mechanically robust structures (not based on free-standing membranes) could pave the way for the realization of on-chip slow-light bio-sensing, active hybrid-silicon optoelectronic devices, or all-optical hybrid-silicon nonlinear functionalities. © 2017 Chinese Laser Press

OCIS codes: (130.5296) Photonic crystal waveguides; (230.5298) Photonic crystals; (230.0230) Optical devices.

https://doi.org/10.1364/PRJ.6.000054

1. INTRODUCTION AND MOTIVATIONS

The tremendous progress achieved in silicon photonics in recent years has now made this research field enter near-to-market applications, with CMOS compatibility as an accelerator. A rich set of passive optical structures including waveguides, microring resonators, filters, and multiplexers/demultiplexers, to name a few, have been demonstrated in silicon-on-insulator (SOI) technology [1–4]. Active optoelectronic structures, including optical modulators, photodetectors, and various configurations towards the realization of light-emitting devices, have also received considerable interest [1,5–7]. Simultaneously, silicon itself cannot provide all the needed functionalities for several reasons—for instance, an indirect band structure, precluding direct efficient light emission, and strong two-photon absorption at telecom wavelengths, hindering the realization of nonlinear functionalities [8]. In this view, the hybrid integration of active materials supplementing silicon physical properties provides an additional degree of freedom that can extend the functionalities of the silicon photonic platform. Electroluminescent or amplifying materials including quantum dots, semiconductor carbon nanotubes [9], doped nanocrystals, erbium-doped organic or inorganic hosts [10,11], as well as second- or third-order nonlinear optical soft materials [12,13] are among the configurations of interest for the realization of integrated optical functions.

The strategy consists of designing structures that maximize the optical power into the added low-index active materials. In a way, this objective is in contradiction with the use of silicon as a material of high optical index, insofar as silicon remains necessary to realize optical waveguides but should not concentrate the main part of the guided optical power. This contradiction is partially lifted by the use of hollow-core waveguides, the so-called slot waveguides [14]. These devices comprise a void core between two Si rails that can be filled by various materials to match the objectives of hybrid-on-silicon integration. In this particular waveguide geometry, the discontinuity of the electric field normal component at the interface between high- and low-index materials is responsible for a strong field compression into the low-index dielectric slot, thus giving rise to enhanced

light–matter interaction. In recent years, several key building blocks have been developed based on these particular silicon waveguides, including directional couplers and microring resonators in all-pass and add-drop configurations [14,15]. Beyond the specificities associated with the partial confinement of light in the low-index material, these works have demonstrated quite remarkable performance in terms of bending losses, propagation losses (~1 dB/cm in TE light polarization around 1.55 μm wavelength), or ring resonator quality factors (around 30,000) [16].

Slot photonic crystal waveguides (SPhCWs) comprise a low-index void between two photonic crystal structures. This way, they can exploit the spatial confinement (slot effect) and pulse compression (slow-light effect) to further enhance light–matter interactions [17]. Furthermore, by bringing the slot modes to the platform of planar crystals, SPhCWs can leverage the engineering knowledge of slow-light modes resulting from the works carried out on (modified) W1 waveguides, especially for the control of light group index and group velocity dispersion (GVD) of Bloch modes [18]. As a result, SPhCW represents an excellent photonic platform for the hybrid integration of novel materials on silicon. However, to take full advantage of the approach, solutions based on the use of non-freestanding membranes should be preferred for practical reasons, among others ensuring mechanical robustness and relaxing planar integration requirements of the added materials [19]. From the waveguiding point of view, a lower vertical index contrast, leaving the oxide BOX underneath, translates in a lower light cone (i.e., smaller bandwidth). This restriction can be mitigated by engineering the optical mode confinement.

The work proposed in this paper is based on slow-light SPhCW engineering and offers an exploration of novel slow-light applications for the hybrid integration of active materials in silicon. We first estimate and optimize the light-confinement properties of SPhCW as a function of the considered slow-light regime. In a second step, we develop an approach allowing the exploitation of the fundamental mode of SPhCW, which minimizes the out-of-plane optical propagation losses. Finally, we show that the use of SPhCWs with corrugated slots in the form of a Bragg comb [20] allows a remarkably wide flat-band slow-light operation of around 60 nm in the telecom range (~1.55 μm wavelength). This approach also opens up a wealth of possibilities for the engineering of the slow modes of SPhCWs. In particular, we show that an adjustment of the geometry of the slot makes it possible to play in a very flexible and quasi-independent manner on the two guided modes of even symmetry of these guides. As a result, the waveguides can be designed to support only two modes of even symmetry in the bandgap of the bulk photonic crystal medium, an unusual and interesting situation for photonic crystal waveguides. Moreover, the spectral deviation between these two modes can also be adjusted in a flexible manner—for example, with a view to exploiting nonlinear optical effects in guided wave configurations (e.g., cross-phase modulation).

2. OPTIMIZATION OF PHC SLOT WAVEGUIDES

Figure 1(a) shows the typical geometry, consisting of an SOI SPhCW. A typical SOI silicon thickness of 260 nm is

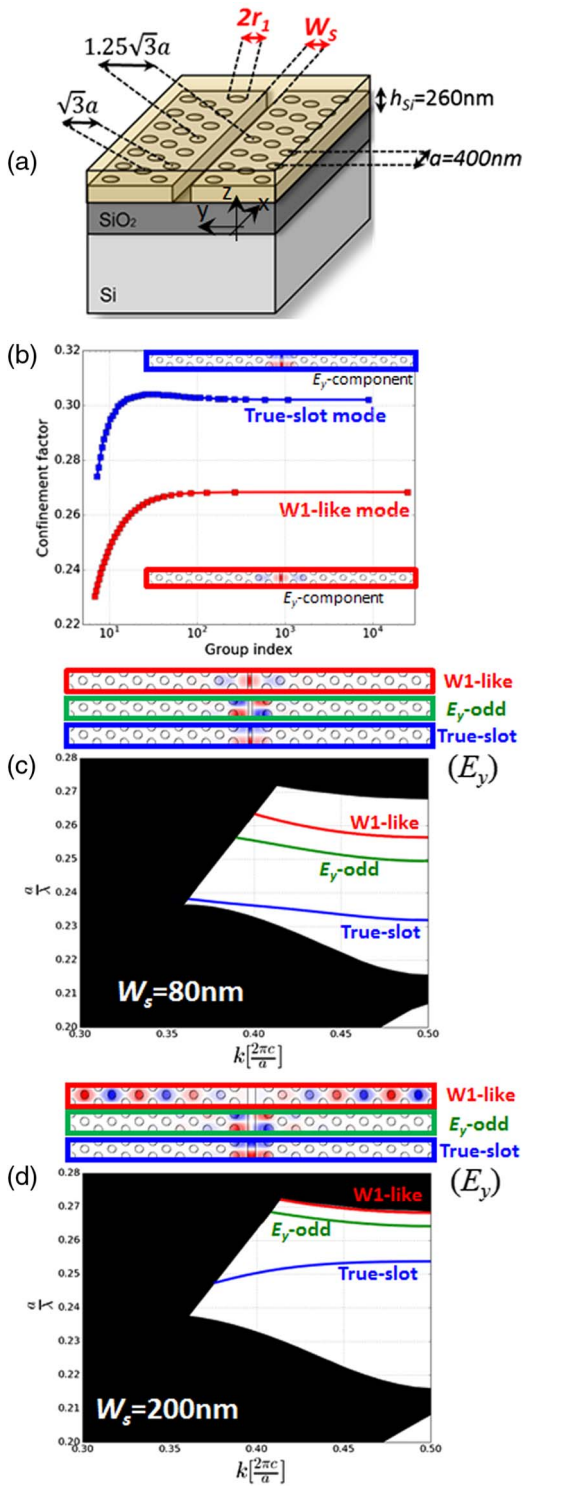

Fig. 1. SOI SPhCW covered by a cladding material of n_{clad} index. (a) Geometry with the parameters shown: $n_{Si} = 3.48$, $n_{SiO2} = 1.44$, $n_{clad} = 1.52$, $r_1 = 120$ nm, $r = 105$ nm (radius of all holes outside the two first rows); (b) influence of the slowing-down factor (n_G) on the confinement properties of SPhCW designed for the integration of materials of index ~1.5: dielectric energy confinement (η_{clad}) of the W1-like and true-slot modes; (c) and (d) dispersion diagrams for $W_S = 80$ nm, $W_S = 200$ nm, respectively. Additionally, insets give the real-space E_y-field component distributions of the three modes at $k = 0.5 \times 2\pi c/a$ in linear scale. Fields are normalized to carry a unitary mode dielectric energy.

considered throughout this work. Compared to a conventional W1 type photonic crystal waveguide, the introduction of a slot in the geometry [of W_S width: see Fig. 1(a)] tends to reduce the effective index of the guiding layer and thus to shift the eigenmodes of the structure towards higher frequencies [17]. In order to compensate this effect, the width between the two central rows of the photonic crystal is extended from $\sqrt{3}a$, the standard value for a W1 PhC waveguide, to $1.25\sqrt{3}a$. In the perspective of the integration of hybrid materials with optical index close to 1.5, a superstrate index $n_{\text{clad}} = 1.52$ is considered, corresponding to a whole class of polymer materials of interest, notably for their nonlinear optical properties around $\lambda = 1.55$ μm [21].

Other works focused on other applications such as electro-optical modulators [22] may also benefit from the approach proposed hereafter. Figures 1(b) and 1(c) show the dispersion diagrams for the two related SPhCWs obtained for a slot width of 80 and 200 nm, respectively. The results presented in this paper have been obtained using three-dimensional plane wave expansion calculation implemented with the MPB software [23]. As expected, the slot width has a very important effect on the dispersion diagram of the waveguide, leading to a significant increase in the frequency of the guide modes in the bandgap of the 2D photonic crystal and to a change in the concavity of certain modes in the first Brillouin zone. In particular, the fundamental mode, the so-called "True slot mode," presents a positive concavity and is preferentially observed in wide slot cases [Fig. 1(c)]. On the other hand, the so-called "W1-like" mode (in analogy with the conventional mode of W1-type photonic crystal guides), appears in the band gap as the directly usable mode of even symmetry for narrow slots [Fig. 1(b)]. As also visible, between these two even-E_y symmetry Bloch modes, SPhCW present an E_y-odd mode. In view of the field maps of the three modes conventionally encountered in SPhCW, it is also observed that the field of the W1-like mode concentrates essentially in both the central slotted region and the second row of holes. The true-slot mode tends to be preferentially confined in the slot and the first row of holes. As sustained by the orthogonal character of the Bloch modes, the field spatial distribution of these two modes thus differs. We shall see later that this property can be used for the engineering of these particular Bloch modes.

From the perspective of the hybrid integration of materials, a key parameter is the spatial overlap (η_{clad}) between the guided modes and the material. Previous works devoted to W1 guides have indicated a progressive spreading of the Bloch mode fields when the wavevector approaches the Brillouin zone edge, that is to say, within the slow-light regime [18]. In this way, these observations could lead to the anticipation of a decrease of η_{clad} for an increase of the light group index (n_G). In order to explore this issue for SPhCW, we have calculated the evolution of η_{clad} in the two configurations previously described along each of the two "W1-mode" and "true-slot" dispersion curves shown in Figs. 1(c) and 1(d). The related result obtained by plotting η_{clad} as a function of light group index (n_G) instead of frequency (through the $n_G(\lambda)$ relationship) is shown in Fig. 1(b). As shown, two trends can be observed. First, a spatial confinement of the fields in the low-index material in the ~26% – ~30% range is obtained for both modes. Another interesting result is the confinement saturation for $n_G > 100$. Although this range of group index values cannot be used practically due to the extrinsic propagation losses coming from the structural roughness of the structures, the observed result shows that slowing down the optical modes does not lead to a lateral field spreading. This result, contrary to the observations in W1 waveguides [18], is caused by the discontinuity of the normal component of the electric field at the low-index/high-index region edges. The optimization of the SPhCW mode properties can thus be carried out by evaluating the confinement of the guided Bloch modes directly at the edge of the Brillouin zone.

Given the confinement properties of SPhCW, the two most important geometric parameters are, as can be seen in Fig. 1(a), the width of the slot (W_S) and the radius of the first row of holes located at both sides of the core of the guide (r_1). Figure 2 depicts the calculated confinement, η_{clad}, for the two even modes as a function of those two geometrical parameters at the edge of the Brillouin zone. These maps show that, for the same dimensions, the confinement factors for the true-slot and W1-like modes are quite different. Thus, the dimension optimization of the waveguides must be conducted according to the targeted mode. Due to the slot influence on the mode effective index values, true-slot and W1-like modes exhibit large confinements for wide ($W_S \sim 180$ nm) and narrow slots ($W_S \sim 100$ nm), respectively. Interestingly, the regions where the confinement is typically greater than

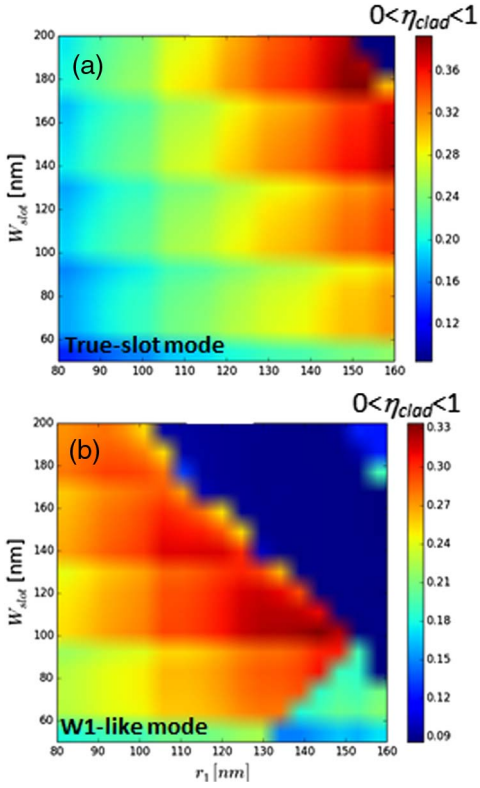

Fig. 2. Dielectric energy confinement in the low-index material (η_{clad}) of silicon SPhCWs studied through the SOI SPhCW configuration described in Fig. 1 at the edge of the Brillouin zone: (a) true slot mode and (b) W1-like mode.

30% extend fairly over ranges of the order of 10–15 nm, that is to say, well within the tolerances of conventional fabrication techniques.

3. CORRUGATED SLOW LIGHT SLOT WAVEGUIDES

In the light of the choices and compromises made at this stage, it appears that the simultaneous exploitation of the two W1-like and True-slot modes is difficult despite their both being interesting in terms of field confinement in the low-index material. In addition, it may also be noted that the presence in the gap of the odd-symmetry mode can also lead to an undesired multimode waveguide operation. To circumvent these difficulties, we use a Bragg-like corrugated slot SPhCW that periodically combines narrow and wide slots [20,24], as shown in Fig. 3(a). The underlying idea is to ensure the confinement of the W1-slot mode by the narrow slot portions while allowing the true-slot mode to spread along its widened portions.

We have verified the accuracy of this hypothesis by calculating the Bloch modes of corrugated slot waveguides. The exact geometry, based on the parameters described in Section 1, includes a cover material with refractive index equal to 1.52, a variable r_1 hole radius, and a slot shape and width described in Fig. 3(a). A preliminary optimization of the double corrugation of the slot allowed us to choose the narrow and wide parts of the slot to be $W_{\mathrm{Sn}} = 50$ nm and $W_{\mathrm{Sw}} = 190$ nm, respectively. We verified that, to maintain locally narrow and wide slots, it was necessary to align the wide portions in front of the lateral holes of the elementary cell of the photonic crystal waveguide [$dx = 0$ in Fig. 3(a)]. Starting from this basic slot structure, we investigated the waveguide modal response by tuning the r_1 parameter.

The remarkable effect of this single parameter is illustrated in Figs. 3(b)–3(d). It can be observed that increasing r_1 from 110 to 140 nm induces an efficient mode-selection process by progressively pulling the E_y-odd mode above the photonic crystal frequency bandgap. As anticipated, it can be observed that the true-slot mode field is stored in the wide part of the slot, while the W1-like one locates in the narrow parts. The differences in behavior of the three modes as a function of r_1 can be explained by their spatial overlap, with the first row of holes in the structure. As the E_y-odd symmetry mode is that of the strongest spatial overlap with the lateral low index holes, it is strongly impacted by the modification of r_1 [Fig. 1(c) and 1(d)]. An increase of r_1 induces a decrease in the effective index of the mode, and therefore an increase in the Bloch mode frequency.

This effect is much less marked for the W1-like mode whose spatial overlap with the first row of patterns is small, while the true-slot mode presents an intermediate situation and is thus also marked by an increase of its band edge frequency. Confinement factors of $\eta_{\mathrm{clad}} = 32.6\%$ and $\eta_{\mathrm{clad}} = 30.3\%$ were calculated for the true-slot and W1-like modes, respectively, considering $r_1 = 140$ nm [configuration in Fig. 3(d)]. These results show that the proposed mode-selection mechanisms do not degrade the light–matter interaction capabilities of SPhCW. It is thus seen that the corrugation of the slot offers interesting possibilities for engineering SPhCW mode selection and makes it possible to obtain dispersion diagrams with only two remaining E_y-even modes in the photonic crystal bandgap, which can naturally be excited from an SOI strip waveguide operating in TE-like polarization. This atypical situation thus allows us to retain only the interesting modes in the bandgap of the photonic crystal and avoid a multimode operation.

It can also be noted from Fig. 3 that the true-slot mode has a very linear frequency dispersion curve, indicating a low group

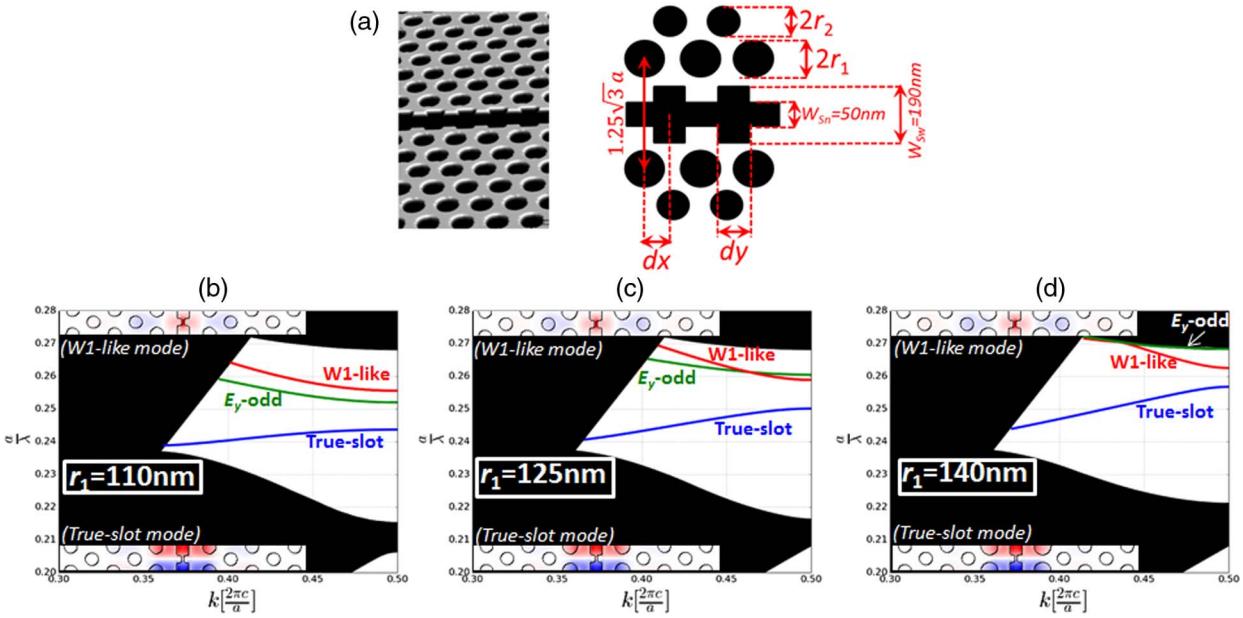

Fig. 3. Bragg-like corrugated SPhCWs. (a) Description of the waveguide geometry; (b)–(d) dispersion diagrams obtained for a 50/150 nm corrugated slot in which wide parts are aligned with the two nearest neighboring holes ($dx = 0$) for $r_1 = 110$, 125, and 140 nm, respectively (all other parameters being identical to the one described in Section 1, including $r_2 = 105$ nm).

velocity dispersion. Since this mode is naturally located very far below the light line, it can be anticipated that the proposed geometry opens the way to dispersion engineering for the exploitation of slow waves and the realization of third-order nonlinear effects by cancellation or near-cancellation of the mode GVD. To go further in this direction, the flexibility of the proposed geometry can be used. The spatial localization of the two modes in the elementary cell of the photonic crystal indeed makes it possible to independently tailor each of the two modes by making local modifications that affect one of the two modes but leaves the other one almost unperturbed. In this idea, we noted that the field of the W1-like mode has a large overlap with the second row of patterns (of radius r_2), whereas this overlap is weaker in the true-slot mode case (see Fig. 3). A modification of r_2 was therefore likely to induce different modifications of the two modes.

We report in Fig. 4 the influence of the r_2 parameter on the frequency of the edge of the Brillouin zone for the two Bloch modes. These calculations were realized by the plane wave expansion method. As visible, an outstanding stability of the true slot mode edge wavelength is noticed when increasing r_2 from 85 to 115 nm, while a decrease of the W1-like mode edge wavelength is observed as a function of r_2, following a nearly linear slope ($\Delta\lambda_{W1-like}/\Delta r_2 \sim -1.45$). It is thus remarked that a very flexible adjustment of the frequency deviation between the two Bloch modes of even symmetry can be achieved by a quasi-independent adjustment of the parameter r_2 with respect to the rest of the structure properties which remain almost unmodified.

The effect of the r_2 parameter on the true-slot mode is a bit more subtle. Although not leading to a significant change in its frequency, we observed that the GVD of the mode (second-order parameter) could be adjusted using this geometrical parameter. Further, it can be observed in Fig. 4(a) that the frequency of the true-slot mode has, in the studied configuration, a very linear portion which is the signature of a low GVD. We have explored this question quantitatively by calculating the classical "flat band slow light" figure of merit introduced in previous works and named the normalized delay bandwidth product (NDPB) [19,25,26]. To quickly summarize earlier discussions, the NDPB factor quantifies the relative spectral width that provides a target group index ($\langle n_G \rangle$) of plus or minus 10% around a considered frequency ($\omega_0 = a/\lambda_0$): NDBP $= \langle n_G \rangle \frac{\Delta\omega}{\omega_0}$. This factor serves in particular to evaluate whether, in addition to a marked slow wave regime, the usable spectral band is not reduced. In other words, the higher the NDBP, the larger the ratio between the bandwidth and the group velocity.

Figure 5 presents the main results of the study we carried out concerning the adjustment of the dispersion properties of the true-slot mode of corrugated SPhCW as a function of the r_2 parameter. Figure 5(a) shows the dispersive properties of a typical configuration (obtained for $r_2 = 115$ nm), namely the

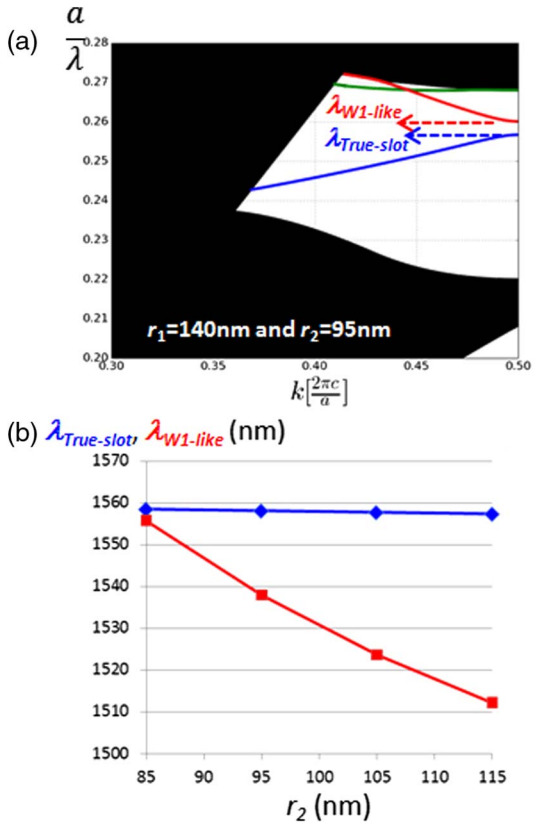

Fig. 4. Strong influence of the r_2 parameter on the frequency splitting between the two even-mode symmetry slot modes: (a) dispersion diagram obtained for $r_1 = 140$ nm and $r_2 = 95$ nm (see Section 1 for a complete description of all other parameters; the two arrows are an identification of the two studied modes); (b) wavelength splitting between the true-slot and W1-like modes as a function of r_2.

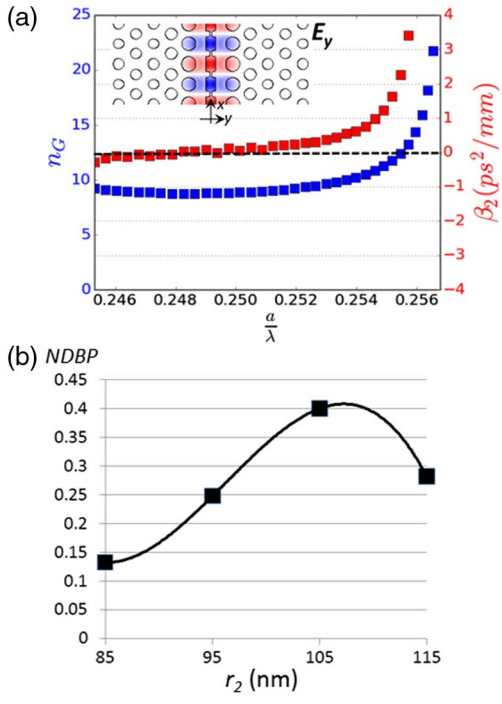

Fig. 5. Adjustment of the dispersive properties of the corrugated SPhCW by the r_2 parameter: (a) group index and GVD proprieties (β_2) for the $r_2 = 115$ nm configuration; (b) evolution of the SPhCW "flat band slow light" normalized delay product of the true slot mode as a function of the diameter of the second row of holes (r_2).

evolution of the group index (n_G) and the GVD (β_2) of the mode as a function of the reduced frequency a/λ. This result confirms the high stability of the group index, leading to a low GVD in a very wide spectral range. Quantitatively, the condition $|\beta_2| < 1$ ps^2/mm is found to hold in an ~60 nm wavelength bandwidth, demonstrating the exceptional potential of corrugated SPhCW as a hybrid integration host of third-order nonlinear materials in which phase-matching conditions often correspond to ensure ultra-low GVD [8]. It can be noticed that moderate group index values are obtained, around $n_G = 10$. However, these values correspond to higher light–matter interaction than in standard slow-light waveguides. Due to the presence of the slot, the light–matter factor $(n_G/n_{\mathrm{mat}})^2$, with n_{mat} the main core waveguide material (here $n_{\mathrm{mat}} \sim 1.5$), indeed scales as $(n_G/1.5)^2$ where it scales as $(n_G/3.5)^2$ in standard guides.

To complete the study, Fig. 5(b) shows the evolution of the NDBP factor as a function of r_2, which we varied between 85 and 115 nm. We observe that very large values of NDBP are obtained and that an optimum as a function of r_2 can be found, so an optimization process depending on the cladding properties or fabrication constraints can be performed in our proposed platform. Our SPhCW exploits the vicinity of the true-slot mode to the low frequencies of the dispersion diagram to yield a remarkably large NDBP exceeding 0.4. This is close to the maximum theoretical value achievable for slow-light photonic crystal modes [27] and a twofold improvement compared to previously reported structures fully covered with active materials, with NDBP ~ 0.2 [19,25,26].

All these results show the versatility and flexibility of the corrugated SPhCWs for the control of the parity of the modes and of their GVD opening a large number of applications requiring light–matter interaction optimization, in particular phase-matching condition for nonlinear functionalities.

4. CONCLUSION AND OUTLOOKS

To conclude, maximizing the interaction between the Si photonic waveguides and the low-index materials surrounding them is crucial for a wide range of applications. In this paper, we show that periodically modulating the width of the center slot of SPhCWs provides an efficient way to independently tailor the properties of the even true-slot and W1-like modes of SPhCWs while maintaining an overlap factor with low-index surrounding medium around 30%. To do so, we simultaneously meet two contradictory requirements in conventional slot waveguides (with a uniform slot): having a wide slot for the even-symmetry mode (true-slot mode) and a narrow slot for the even mode present in the gap (W1-like mode). The indentation of the slot in fact forces the two modes to position themselves opposite the wide and narrow parts of the slot. The fairly differentiated localization of the electric field profiles of the two modes makes it possible to perform structural modifications (r_1 and r_2 radii of the first two rows of holes) having distinct effects on each of the two modes. Another advantage of this approach is to allow a very efficient rejection of the odd mode out of the photonic crystal bandgap. This results in an unusual situation, consisting of a photonic bandgap guiding platform with only two slot modes of even symmetry. The optimized SPhCW exhibits an NDBP larger than 0.4, close to the theoretical limit for slow-light photonic crystal modes [27].

We believe that the corrugated slow-light slot waveguides presented in this work offer interesting prospects for the integration of active materials on silicon. The flexibility offered by the introduction of slot corrugation, in terms of engineering of parity of modes and control of the dispersion, bring in appreciable degrees of freedom for the reinforcement of the light–matter interactions or the preparation of the needed phase-matching conditions to exploit nonlinear optical effects.

REFERENCES

1. L. Vivien and L. Pavesi, *Handbook of Silicon Photonics* (CRC Press, 2013).
2. G. Li, J. Yao, H. Thacker, A. Mekis, X. Zheng, I. Shubin, Y. Luo, J.-H. Lee, K. Raj, J. E. Cunningham, and A. V. Krishnamoorthy, "Ultralow-loss, high-density SOI optical waveguide routing for macrochip interconnects," Opt. Express **20**, 12035–12039 (2012).
3. W. Bogaerts, P. De Heyn, T. Van Vaerenbergg, K. De Vos, S. K. Selvaraja, T. Claes, P. Dumon, P. Bientsman, D. Van Thourhout, and R. Baets, "Silicon microring resonators," Laser Photon. Rev. **6**, 47–73 (2012).
4. D. Bernier, X. Le Roux, A. Lupu, D. Marris-Morini, L. Vivien, and E. Cassan, "Compact, low cross-talk CWDM demultiplexer using photonic crystal superprism," Opt. Express **16**, 17209–17214 (2008).
5. D. Marris-Morini, L. Virot, C. Baudot, J.-M. Fédéli, G. Rasigade, D. Perez-Galacho, J.-M. Hartmann, S. Olivier, P. Brindel, P. Crozat, F. Bœuf, and L. Vivien, "A 40 Gbit/s optical link on a 300-mm silicon platform," Opt. Express **22**, 6674–6679 (2014).
6. Z. Liu, J. Kakande, B. Kelly, J. O'Carroll, R. Phelan, D. J. Richardson, and R. Slavík, "Modulator-free quadrature amplitude modulation signal synthesis," Nat. Commun. **5**, 5911 (2014).
7. L. Virot, P. Crozat, J.-M. Fédéli, J.-M. Hartmann, D. Marris-Morini, E. Cassan, F. Boeuf, and L. Vivien, "Germanium avalanche receiver for low power interconnects," Nat. Commun. **5**, 4957 (2014).
8. J. Leuthold, C. Koos, and W. Freude, "Nonlinear silicon photonics," Nat. Photonics **4**, 535–544 (2010).
9. E. Gaufrès, N. Izard, X. Le Roux, S. Kazaoui, D. Marris-Morini, E. Cassan, and L. Vivien, "Optical microcavity with semiconducting single-wall carbon nanotubes," Opt. Express **18**, 5740–5745 (2010).
10. L. Agazzi, J. D. B. Bradley, M. Dijkstra, F. Ay, G. Roelkens, R. Baets, K. Wörhoff, and M. Pollnau, "Monolithic integration of erbium-doped amplifiers with silicon-on-insulator waveguides," Opt. Express **18**, 27703–27711 (2010).
11. M. Zhang, W. Zhang, F. Wang, D. Zhao, C. Qu, X. Wang, Y. Yi, E. Cassan, and D. Zhang, "High-gain polymer optical waveguide amplifiers based on core-shell $NaYF_4$/$NaLuF_4$: Yb^{3+}, Er^{3+} NPs-PMMA covalent-linking nanocomposites," Sci. Rep. **6**, 36729 (2016).
12. T. Wang, N. Venkatram, J. Gosciniak, Y. Cui, G. Qian, W. Ji, and D. T. H. Tan, "Multi-photon absorption and third-order nonlinearity in silicon at mid-infrared wavelengths," Opt. Express **21**, 32192–32198 (2013).
13. E. Timurdogan, C. V. Poulton, M. J. Byrd, and M. R. Watts, "Electric field-induced second-order nonlinear optical effects in silicon waveguides," Nat. Photonics **11**, 200–206 (2017).
14. P. A. Anderson, B. S. Schmidt, and M. Lipson, "High confinement in silicon slot waveguides with sharp bends," Opt. Express **14**, 9197–9202 (2006).
15. C. A. Barrios, "Optical slot-waveguide based biochemical sensors," Sensors **9**, 4751–4765 (2009).
16. W. Zhang, S. Serna, X. Le Roux, C. Alonso-Ramos, L. Vivien, and E. Cassan, "Analysis of silicon-on-insulator slot waveguide ring resonators targeting high Q-factors," Opt. Lett. **40**, 5566–5569 (2015).
17. A. Di Falco, L. O'Faolain, and T. F. Krauss, "Dispersion control and slow light in slotted photonic crystal waveguides," Appl. Phys. Lett. **92**, 083501 (2008).

18. T. Krauss, "Slow light in photonic crystal waveguides," J. Phys. D **40**, 2666–2670 (2007).
19. S. Serna, W. Zhang, P. Colman, X. Le Roux, J. R. Coudevylle, L. Vivien, and E. Cassan, "Experimental investigation of top cladding on properties of silicon slotted photonic crystal waveguides," IEEE J. Sel. Top. Quantum Electron. **22**, 305–311 (2016).
20. C. Caer, X. Le Roux, V. K. Do, D. Marris-Morini, N. Izard, L. Vivien, D. Gao, and E. Cassan, "Dispersion engineering of wide slot photonic crystal waveguides by Bragg-like corrugation of the slot," IEEE Photon. Technol. Lett. **23**, 1298–1300 (2011).
21. S. Serna, P. Colman, W. Zhang, X. Le Roux, C. Caer, L. Vivien, and E. Cassan, "Experimental GVD engineering in slow light slot photonic crystal waveguides," Sci. Rep. **6**, 26956 (2016).
22. X. Zhang, A. Hosseini, S. Chakravarty, J. Luo, A. K. Y. Jen, and R. T. Chen, "Wide optical spectrum range, subvolt, compact modulator based on an electro-optic polymer refilled silicon slot photonic crystal waveguide," Opt. Lett. **38**, 4931–4934 (2013).
23. S. G. Johnson and J. D. Joannopoulos, "Block-iterative frequency-domain methods for Maxwell's equations in a planewave basis," Opt. Express **8**, 173–190 (2001).
24. C. Caer, X. Le Roux, and E. Cassan, "Enhanced localization of light in slow wave slot photonic crystal waveguides," Opt. Lett. **37**, 3660–3662 (2012).
25. T. Baba, "Slow light in photonic crystals," Nat. Photonics **2**, 465–473 (2008).
26. R. Hao, E. Cassan, H. Kurt, J. Hou, X. Le Roux, D. Marris-Morini, L. Vivien, D. Gao, Z. Zhou, and X. Zhang, "Novel kind of semislow light photonic crystal waveguides with large delay-bandwidth product," IEEE Photon. Technol. Lett. **22**, 844–846 (2010).
27. R. Hao, E. Cassan, X. Le Roux, D. Gao, V. K. Do, L. Vivien, D. Marris-Morini, and X. Zhang, "Improvement of delay-bandwidth product in photonic crystal slow-light waveguides," Opt. Express **18**, 16309–16319 (2010).